Title

Digital Fabrication and Integration of a Flexible Wireless Sensing Device

Journal

IEEE Sensors Journal, 17(21)

ISSN

1530-437X

Authors

Mei, Ping
Krusor, Brent
Schwartz, David E
et al.

Publication Date

2017

DOI

10.1109/jsen.2017.2753740

Peer reviewed

Digital Fabrication and Integration of a Flexible Wireless Sensing Device

Ping Mei, Brent Krusor, David E. Schwartz, Tse Nga Ng, George Daniel, Steve Ready, and Gregory L. Whiting

***Abstract*— In this paper, we combine high functionality c-Si CMOS and digitally printed components and interconnects to create an mostly printed integrated electronic system on a flexible substrate that can read and process multiple discrete sensors. Our approach is to create an integrated platform for the fabrication of mechanically flexible sensor tags that can be powered and interrogated wirelessly, precluding the need of a separate on-board power source. The high level system design is aimed at minimizing the number of non-printed components and reducing power consumption to enable energy harvesting from the RF field. Digital fabrication of these systems requires a range of materials, feature sizes, and electrical characteristics. In order to integrate the various printed components on a single substrate, we developed an integrated printer to accommodate a range of inks for printing the antenna, different types of sensors, chip interconnects, and wiring. For chip attachment to the flexible substrate, a method of integrating the die within the thickness of the substrate was developed. With proper system design and fabrication, a complete integrated tag for wireless sensing of temperature, strain, and touch was demonstrated. Our approach facilitates customization to a wide variety of sensors and user interfaces suitable for a broad range of applications including remote monitoring of health, structures, and the environment.**

***Index Terms*— Hybrid integrated circuits, digital printing, flexible printed circuits, flexible electronics, printed sensor, strain sensor, touch sensor.**

I. Introduction

MECHANICALLY flexible sensor systems can be used to address a broad array of application areas including biomedicine, wearable electronics, transportation, and structural monitoring. Printing is an attractive fabrication method for flexible electronic systems as it enables coverage over large areas, and is typically a low-temperature process, allowing for integration with common plastic substrates [1]–[5]. In addition, printing is a direct patterning process that enables facile customization and, in contrast with typical subtractive methods, avoids damaging sensitive organic or biochemical materials. Printing provides a deposition approach suitable for fabrication of a wide range of sensors, and for integration with other componentry, such as signal processing electronics [1], [2], [6]–[11].

Ideally, for distributed sensing applications, these systems should be standalone, and include all of the components necessary to perform a particular sensing task, and should be capable of disseminating sensor data to networked devices for further analysis [12], [13]. While wireless transmission of the sensor data for the distributed system is highly desirable, it can be difficult to implement in printed systems due to the performance limitations of printed circuits, the power consumption of the radio, and the antenna impedance matching requirements. Providing on-board power for a flexible, printed system is a particular challenge. Printed batteries can be incorporated into the system, but have limited capacity in thin form factors, necessitating eventual replacement or recharging. To overcome this issue, energy harvesting approaches can be used, including using energy provided by thermal [14], [15], optical [16], mechanical [17], acoustic [18] or radiofrequency (RF) [19] sources. RF energy harvested from a dedicated source is of particular interest as it allows for a simplified system that can function in a wide range of environments, and can be addressed using readily available readout devices.

Fully printed electronics can provide excellent flexibility and customizability, as well as the potential for low-cost fabrication and the ability to address large-area applications. However, due to materials properties and available feature sizes, printed circuits are currently not suitable for functions such as RF harvesting/data transmission and high-resolution analog-to-digital conversion [20]. Conventional electronics mounted on flexible printed circuit boards provide high performance but have reduced mechanical flexibility and may not be compatible with additive printing techniques. As such, incorporation of silicon dies or packaged chips into a printed platform is a promising approach to enable high performance without significantly compromising mechanical flexibility, cost, or the rapid customizability of printed systems [21].

Here we describe a passively-powered flexible sensor platform using a hybrid combination of digitally-printed sensors alongside a data-logging chip. The system is demonstrated using strain and touch sensors, which may be useful for applications such as structural health monitoring. The sensor system is composed primarily of printed components, including sensors, antenna, and interconnects. A packaged or bare-die RF chip, capable of being powered wirelessly using a dedicated reader device, is mounted on the flexible substrate, and interconnected to the printed components through the use of printing techniques. Such devices typically require multiple passive components, particularly for matching the antenna

Manuscript received July 18, 2017; revised September 8, 2017; accepted September 10, 2017. Date of publication September 18, 2017; date of current version October 11, 2017. This work was support by the FlexTech Alliance ‘under Contract RFP14-166. The associate editor coordinating the review of this paper and approving it for publication was Prof. Danilo Demarchi. *(Corresponding author: Ping Mei.)*

P. Mei, B. Krusor, D. E. Schwartz, G. Daniel, and S. Ready are with the Palo Alto Research Center, Palo Alto, CA 94304 USA (e-mail: ping.mei@parc.com).

T. N. Ng was with the Palo Alto Research Center, Palo Alto, CA 94304 USA. She is now with the Department of Electrical and Computer Engineering, University of California at San Diego, La Jolla, CA 92093 USA.

G. L. Whiting was with the Palo Alto Research Center, Palo Alto, CA 94304 USA. He is now with Department of Mechanical Engineering, University of Colorado Boulder, Boulder, CO 80309 USA.

Digital Object Identifier 10.1109/JSEN.2017.2753740

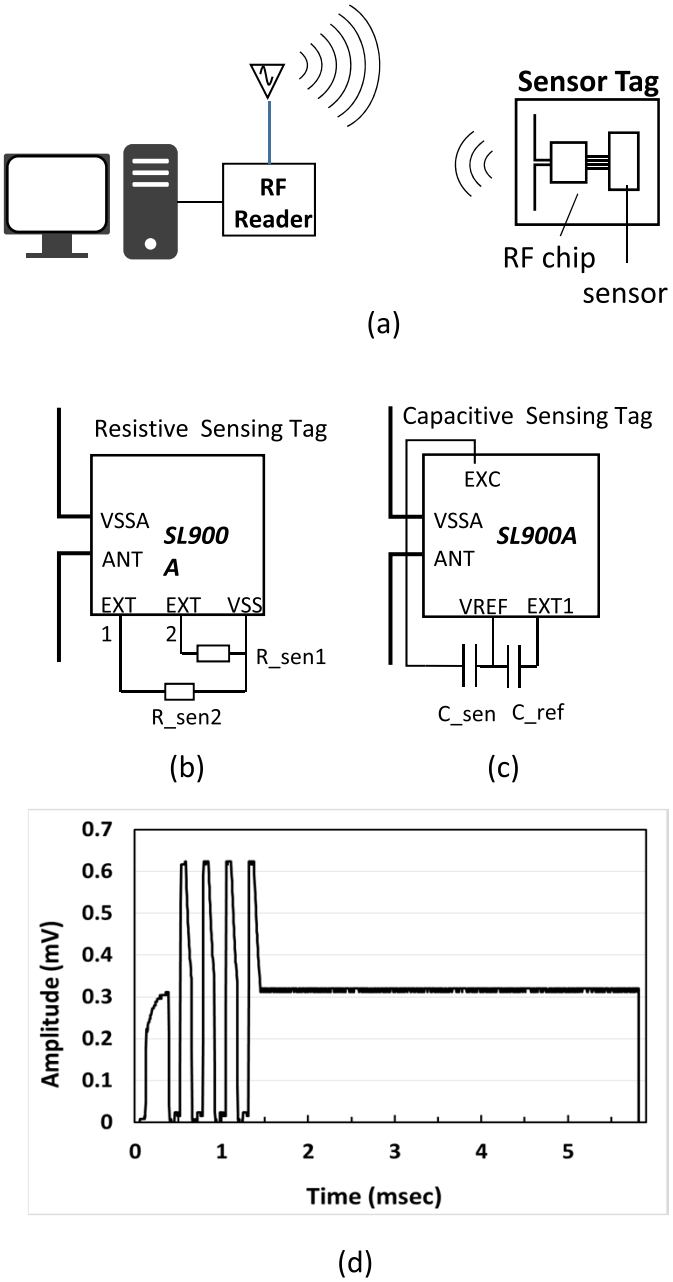

Fig. 1. (a) Illustration of passive sensor tag to reader communication. (b) and (c) Schematic of resistive and capacitive sensor tag using SL900A RF chip. (d) Waveform generated at EXC pin of SL900A.

impedance to the chip input. Here, we focus on minimizing the component count, particularly through RF design of printed conductors, in order to provide as simple a functional system as possible, which is important for reliability and low manufacturing cost.

II. Wireless Sensor System Design

Our system design is based on three main considerations: using minimal power consumption for energy harvesting, being able to read multiple sensor inputs, and printing as much of the circuit as possible to minimize the number of discrete components needed. In this study, we designed and constructed a remote sensor system as illustrated in Fig.1.

TABLE I
Comparison of Various Digital Printing Properties

	Ink Jet	Aerosol	Extrusion
Viscosity (Pa s)	$10^{-4} – 10^{-2}$	$10^{-2} – 1$	$1 – 10^{2}$
Minimum Feature Size:			
Line width	~60 μm	50-60 μm	>500 μm
Line gap	~30 μm	~40 μm	>300 μm
Thickness	200 – 300 nm	~ 1μm	>10μm

The system hardware includes a computer, a UHF reader, and the sensor tag itself. The SL900A data-logger chip from AMS was selected from available RF communication chips as the core component of the sensor tag. In our design, the SL900A was operated in fully-passive mode which does not require a battery to supply power. Instead the system is be powered directly via the RF field provided by the external UHF reader antenna [22], eliminating the need for an on-board power supply. The SL900A chip includes an internal temperature sensor and has two ADC converter channels to read external sensors. Fig 1 (b) shows a schematic of a two-channel resistive sensor connection to the chip. One channel (EXT 1) measures a resistive value, while the other channel (EXT 2) measures the conductance of the connected resistor. Fig 1(c) shows the configuration for capacitive sensing. In this design, antenna, resistors and capacitors are printed. The only discrete components to be mounted on the substrate are the SL900A and optionally a reference capacitor. Powered by reader's RF signal, the chip can generate four 600 mV AC pulses at about 3 kHz for an AC measurement as shown in Fig 1(d) (waveform as measured on the EXC pin during an RF excitation).

III. Integrated Printing and Chip Attachment

A. Integrated Digital Printing

Digital, additive printing of electronic materials allows rapid, highly-customizable fabrication. More complex functionality can be achieved by printing interconnects between silicon ICs and printed active and passive components, to combine the advantages of flexible printed devices with the high performance of silicon chips. This approach typically requires the use of multiple printing techniques, which use inks with a wide range of viscosities to be deposited side-by-side onto the substrate at various resolution and thickness. Table I lists the range of viscosity, typical minimum feature size and thickness for ink-jet, aerosol and extrusion printing methods. To avoid the complexity and yield challenges associated with using multiple tools to build these hybrid systems, we have developed an integrated printer that includes a range of digital deposition approaches. Fig 2 shows a photo of the multi-material printing system, which comprises an ink-jet head, two auger-type extrusion tools, and an aerosol-jetting tool, along with a substrate stage with precision motion control of x, y, z, ϑ and cameras to enable registration of printed layers.

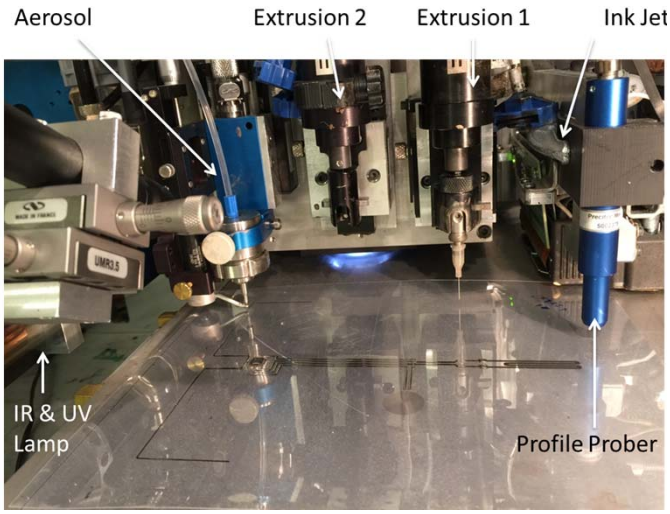

Fig. 2. Photograph of an integrated digital printing system.

In addition, our integrated printing system is equipped with an UV LED lamp and photonic heater to provide inline curing and drying of printed materials. This system enables multiple divergent materials to be patterned and formed into a sensor tag.

Ink-jet printing allows for deposition of an ink of viscosity in the range of 10^{-4} to 10^{-2} Pa s. The typical resolution of a jetted silver-nanoparticle ink is about a 60 μm in line width and 30 μm in line spacing. This deposition method can be used to create electrodes with a narrow gap, such as the double-coiled capacitive sensor shown in Fig 6 (a).

The ink viscosity for pneumatic aerosol-jet is higher than that for ink-jet, in the range of 0.01 to 1 Pa.s. Due to the higher viscosity, the thickness of the printed traces is larger ($\sim$1 μm compared with $\sim$300 nm from ink-jet). We have used aerosol printing to make fine pitch connections between an RF chip to interconnection paths as shown in Fig 3 (b).

Extrusion printing can be used for materials with a high viscosity (1-100 Pa.s). Typical line width and line spacing for an extruded silver-nanoparticle ink are about 500 μm and 300 μm, respectively, depending on the gauge of the extrusion needle and the print speed. The thickness of the printed trace is on the order of 10 μm, leading to reduced trace resistance. Extrusion printing can be also used for resistive strain sensors using a carbon ink. Fig 7 (a) shows an extruded Ag antenna as well as carbon strain sensors.

B. Chip Attachment

Integration of the sensor tag includes mounting and electrically connecting the RF chip on the flexible substrate. Distinct approaches to mounting and interconnecting bare-die and packaged versions of the SL900 have been developed. The packaged chip has surface-mount pads in a plastic quad-flat no-leads carrier, with a pad size of 400 μm by 355 μm and pad-to-pad spacing of 800 μm. This type of package can be readily mounted on the flexible substrate using anisotropic conductive film (ACF), with a proper temperature and pressure (Fig 8 (a)) [23], [24]. The bare-die(unpackaged) version offers a smaller form factor and, especially if thinned,

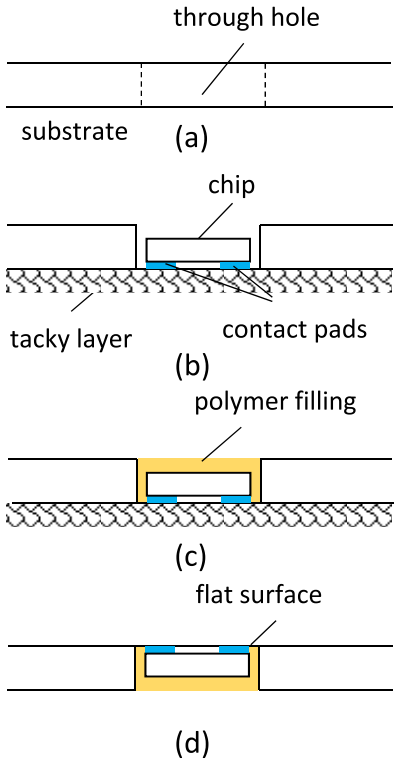

Fig. 3. Illustration of bare die mounting method with the surface of the die flush with the substrate: (a) cut off a through hole through substrate; (b) place chip on a tacky layer; (c) polymer filling; and (d) remove tacky layer and complete the process.

enhanced mechanical flexibility of the resulting device [25]. However, the contact pads on the bare die are typically small, often $<$100 μm square, and difficult to bond with this method because of the large size of the conductive particles in typical ACFs. Printing offers an alternative fabrication method to achieve high density and low resistance interconnections [21]. Conventional bonding processes, such as wire bonding, can be replaced with the directly printed metal interconnect. One challenge with this approach is that it is difficult to maintain continuous interconnect traces from the substrate over the chip's step-edge and onto the contact pads. This can be mitigated by planarizing the step edge to allow for interconnection.

To avoid the step edge, we developed a chip-mounting method in which the surface of the chip is flush with the substrate as shown in Fig 3. The process starts with a flexible substrate such as polyethylene naphthalate (PEN) with a thickness of 150 μm. The substrate may have circuit interconnects printed with a pre-identified location for the chip. As illustrated in Fig 3(a), a region of the substrate of the same size as the bare die is removed using a laser. In a next step (Fig 3(b)), the substrate is placed on a flat article with a tacky upper surface. The tacky layer provides a tight seal against the surface of the chip and the surface of the substrate around the cut off region, and this layer can be removed after the process. In this experiment, we use polydimethyisiloxane (PDMS) for the tacky layer. As shown in Fig 3(b),the chip is placed into the cut off region with its contact surface against the tacky layer. We have thinned down the chip using standard wafer grinding and polishing techniques to about 80 μm, making the

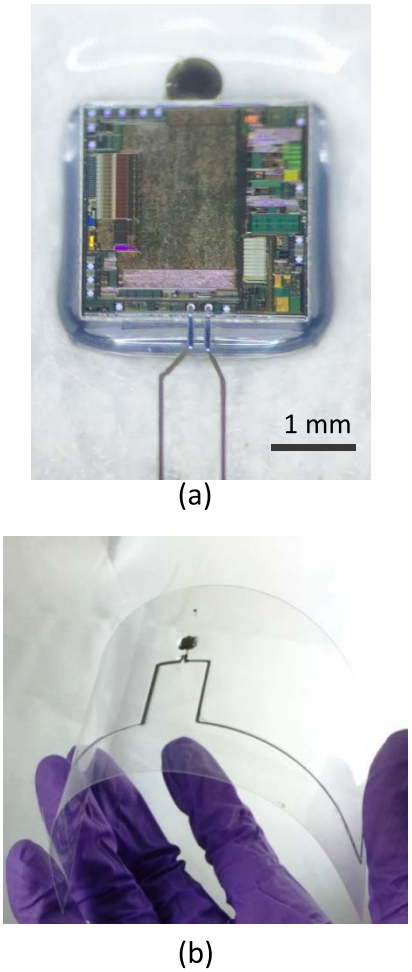

Fig. 4. (a) A microscope image of the mounted SL900A bare die. (b) Photograph of a flexible antenna and a bare die on a sensor tag.

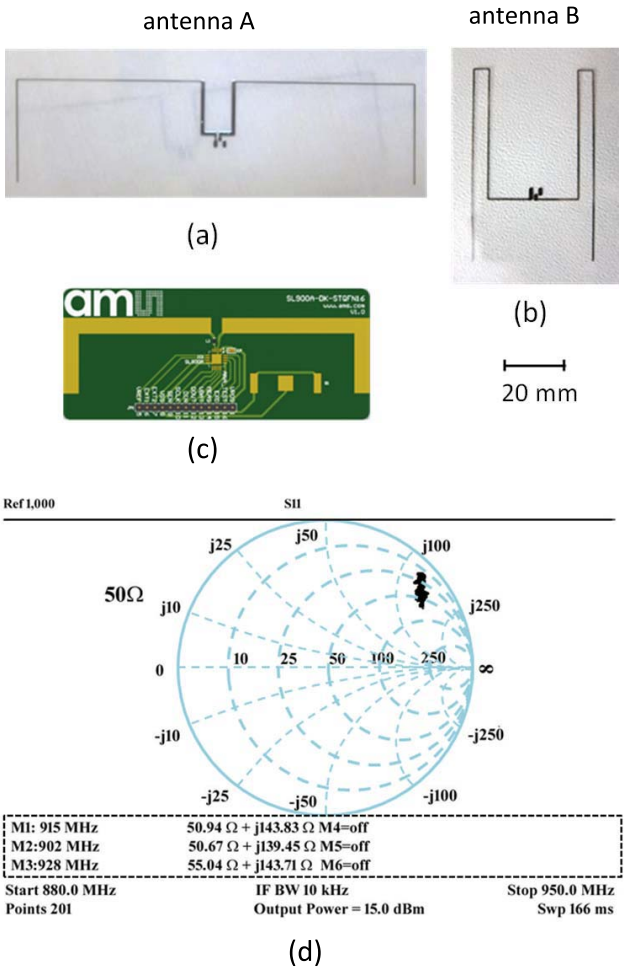

Fig. 5. (a) and (b) Printed antennas of two different designs. (c) Antenna on PCB from AMS development kit. (d) Smith chart of the impedance measurements of antenna (a).

chip thinner than the substrate. As shown in Fig 3(c), a filler adhesive is added to the backside and around the side wall of the die. The adhesive can be UV curable polymer. After the polymer is cured, the chip is fixed in place and the tacky layer is removed leaving the surface of the filler and the chip flush with the substrate surface. Fig 3(d) shows he substrate which has been turned over such that the chip contact surface (with circuits/traces on the substrate) is now facing up. With the die surface flush with the substrate, high-resolution patterning can be readily performed to construct conductive connections between the die and the circuit on the substrate.

Fig. 4 (a) shows a microscope image of the mounted SL900A bare die which is connected to the antenna printed on the substrate by aerosol-jet printing of a silver nanoparticle ink. The pad size is 100 μm by 100 μm and the pad-to-pad spacing is 200 μm.

Although the die is rigid, because of its small size, the tag can be bent with a diameter below 30 mm (Fig 4(b)), showing that functionality was unaffected by this bending exercise.

IV. Results & Discussion

A. Printed Antenna

In the integrated sensor tag shown in Fig 8 (a), the antenna was designed to operate at the reader's frequency of 915 MHz, and to match the impedance of the antenna ports on the packaged chip. In the commercial SL900A development kit, the chip is mounted on a PCB with antenna as shown in Fig. 5(c). A 39-nH inductor is used to enable matching the RF chip input impedance of 31–320j Ω. For our sensor tags, we explored various types of antenna designs in order to match the input impedance of the RF chip without the need for a separate inductor, in order to minimize the number of components on the substrate, and allowing as much of the complete system to be printed directly from liquid inks as possible.

The design of an antenna is facilitated with a software package to simulate the impedance for a given antenna. The shape and dimension of an antenna, and material parameters such as substrate thickness and dielectric constant, silver trace thickness and conductivity of a designed antenna are used as inputs for the simulation. The goal is to select printable antenna designs resulting in minimal impedance mismatch between the designed antenna and the input impedance of chip SL900A. Fig 5 (a) and (b) show two of the printed antennas, A is similar to a typical dipole antenna and B is a simple meander structure, both of them have a total antenna length of about 250 mm. Table II shows the dimensions of the antennas

TABLE II
ANTENNA DIMENSION

Type	Substrate & Conductor	Total Length	Width	Thickness
Antenna A	PEN/Silver	250 mm	0.5 mm	10 μm
Antenna B	PEN/Silver	250 mm	0.5 mm	10 μm
Dev Kit	PCB/Copper	130 mm	5 mm	35 μm

of Fig 5. Fig 5(d) shows a Smith chart plot of the measured impedance of antenna A. The real and imaginary part of the impedance for antenna A at 915 MHz is about 50 Ω and 143 Ω respectively. The real part of the impedance matches the input impedance of the RF chip, but the imaginary part is does not. For antennas B, The real and imaginary part of the impedance is about 34 Ω and 113 Ω respectively (Smith chat not shown), a more significant mismatch to the input impedance than observed with design A. However, in both cases it was noted experimentally that the performance of the reading response of the chip was adequate for data communication within a distance of 15 cm.

The performance of the antennas was evaluated by measurement of the reading responses of different antenna designs. Antenna radiation pattern and signal strength depend on various factors including surrounding materials, antenna shapes, and orientation. In order to have a good comparison, all substrates are laid flat on a wood surface with antenna arms parallel to the reader antenna in the same environment. The measurement was performed using an AMS Radon reader 15 cm from the tag. The reader output power at 915 MHz is ∼30 dBm. To evaluate the RF communication strength of the sensor tags, the number of successful sensor responses during a time interval of 120 seconds was repeatedly counted over 10 times. The average responses from the stock PCB antenna that included a separate inductor is about 850. Antenna A with no additional inductor gave an average count of 900 responses, which is about 5% improved from that of the PCB antenna. With antenna B, an average count of 300 responses was measured. The improved reading response count of antenna A is likely due to better impedance matching of antenna A relative to B.

B. Printed Carbon Strain Sensor

The serpentine-type strain sensors are designed with targeted resistance range of 50 kΩ to 2 MΩ, compatible with the internal reference resistor of the chip (Fig 8 (a)). The extruded carbon ink is formed by mixing a low-conductivity carbon-based ink (Creative Materials 112–47) with a high-conductivity carbon-based ink (Creative Materials 112–48) with weight ratio 5:2 in order to bring the resistance into the targeted range. Showing in Fig. 8 (a), a printed carbon strain sensor is connected to extruded silver traces. The total length of the serpentine carbon line is about 140 mm, the line width is about 1 mm, and the height is about 20 μm.

Fig. 6 (a) shows resistance change when the carbon strain sensor is under compressive and tensile bending conditions with various bending radii ranging from 500 mm to 90 mm. After each bend at a given radius, the sensor is relaxed to its natural position and the resistance value (as shown in black) is observed to return to the initial value.

The gauge factor of the carbon strain sensor is extracted from a plot of the relative resistance change as a function of strain as shown in Fig 6(b). The resistance change is relative to the resistance at its nature state. The strain value is calculated according to Equation (1),

$$strain \approx \frac{d_f + d_s}{2R} \tag{1}$$

for $d_f \gg d_s$. Here d_f and d_s is the thickness of the substrate (150 μm) and carbon resistor (∼20 μm) respectively. R is the bending radius.

In this bending range the gauge factor, which is the slope of the plot of ΔR/R vs strain, is ∼66 in both tensile and compressive bending directions. The carbon strain sensor's response is not linear under small-diameter bending, especially for tensile strain. This effect is not ameliorated by dielectric encapsulation to enhance adhesion of the carbon ink to the substrate, and may be attributed to a change in the internal structure of carbon based material [26].

C. Printed Touch Sensor

As shown in the schematic in Fig 1 (c), a capacitance change can also be read by the SL900A chip, which can be used for touch sensing. Shown in Fig 7(a) are two identical capacitors made using an inkjet-printed silver-nanoparticle ink. Each capacitor is formed by double wrapped coils (14 loops), each coil is designed according to spiral Equation (2):

$$r = ae^{\theta \cot b} \tag{2}$$

in which r is the radius of each turn of the spiral, b is a constant, determining the density of a coil. Parameter b is chosen such that the distance between each turn is about 360 μm. Parameter a is a constant for the outer dimension of the coil. For the second coil, r2 = r1+180μm. The printed trace is 80 μm wide, and the gap between the two coils is therefore about 100 μm. When an object touches, or is placed near the gap between the two coils, there is a change in capacitance associated the permittivity change. The size of the gap is an important design parameter. If the gap is too small, the fringe field between the two conductors will be more concentrated at the surface of the substrate and less sensitive to a finger touch. On the other hand, if the gap is too large, the fringe field will be too weak near the surface. Table III shows experimental data indicating the capacitance change from the coils with and without a finger touch at different measurement frequencies. In this experiment, the coils were covered by a thin (90 μm) sheet of paper to protect the coil from rubbing. Due to dielectric dispersion, the capacitances decrease at higher frequency. Upon finger contact, the change in capacitance is larger when the frequency is lower. At 1 kHz (SL900A measurement frequency), a finger touch causes a 10% change in capacitance, which can be readily detected by an external circuit. It is noticed that the capacitance change is sensitive to touch pressure and skin moisture. During a measurement, the capacitive sensor is excited with a

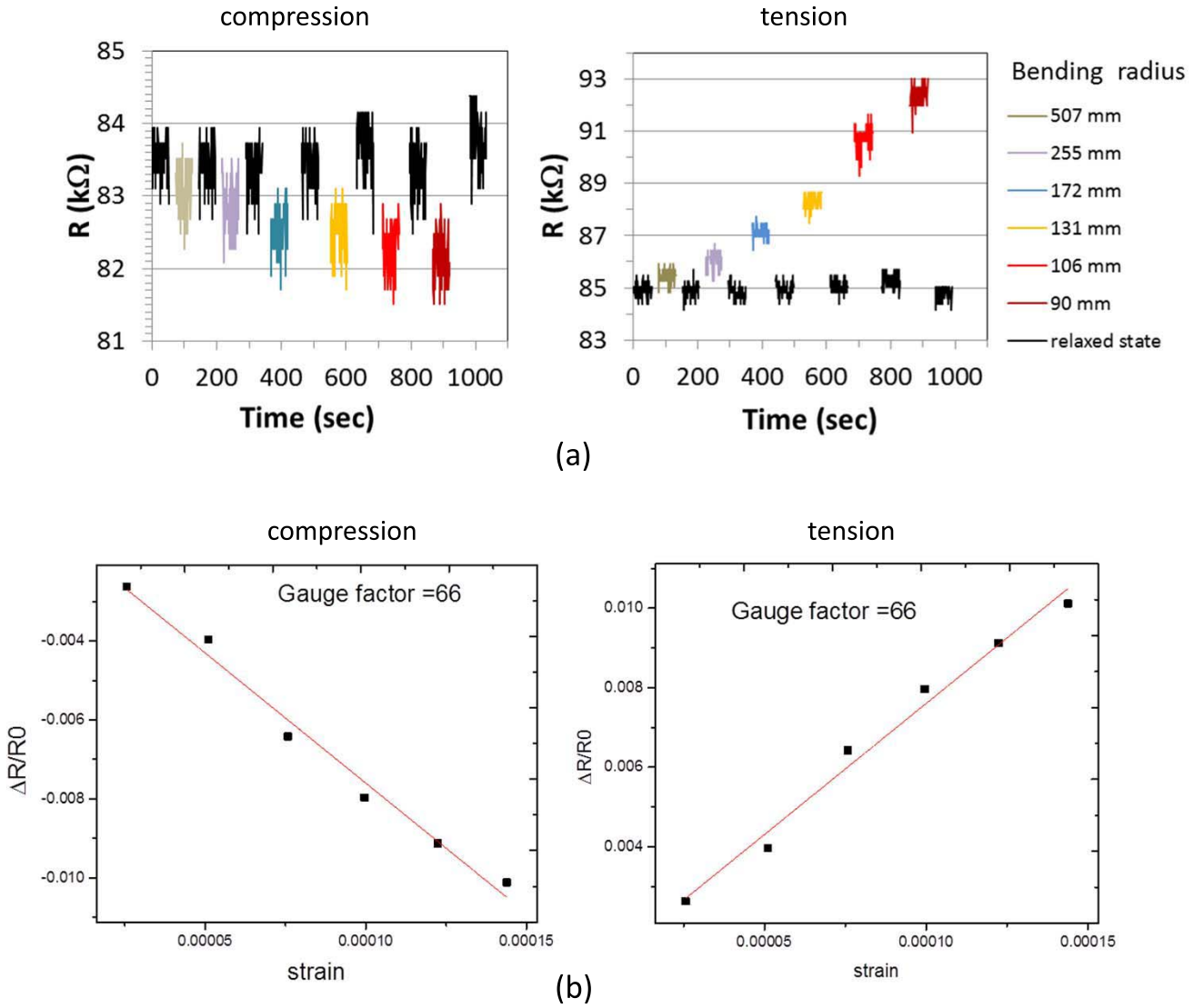

Fig. 6. (a) Time sequence of bending test, showing resistance reading when the carbon strain sensor was under compressive and tensile bending conditions with various bending radii. (b) Relative resistance change as functions of strain for compressive and tensile bending, respectively.

TABLE III
CAPACITANCE OF DOUBLE LOOPED COIL

Frequency of Measurement	Capacitance without Touch	Capacitance with Finger Touch	% of C Change
1 kHz	42 pF	46 pF	10%
500 Hz	54 pF	62 pF	15%
100 Hz	0.13 nF	0.15 nF	15%

square wave signal around the reference voltage VREF (as shown in Fig 1 (d)). The measured voltage at the sensor node is:

$$V_{EXT1} = V_{REF}\frac{C_{SEN}}{C_{SEN}+C_{REF}} \quad (3)$$

When the reference voltage V_{REF} is constant while the capacitance of the sensing capacitor C_{SEN} or reference capacitor C_{REF} increases, the voltage measured at input sensor node 1 changes according to Equation (3). Fig 7 (b) shows the sensor readout data from the SL900A chip. At time t_1 and t_3, a finger touch on the sensing capacitor causes a positive capacitance change of ~40% relative to the reference capacitor. At t_2, when a finger is placed on the reference capacitor, a decrease in capacitance of the reference capacitor versus the sensing capacitor is observed. Since the amount of increase in the reference capacitance only affects the denominator in Equation (3), the decrease in the voltage at the sensor node is not as large as the change at time t_1 and t_3.

D. Integrated Sensor System With Strain and Temperature Sensors

Shown in Fig 8 is an example of complete system made through integration of a c-Si CMOS (SL900A chip) with

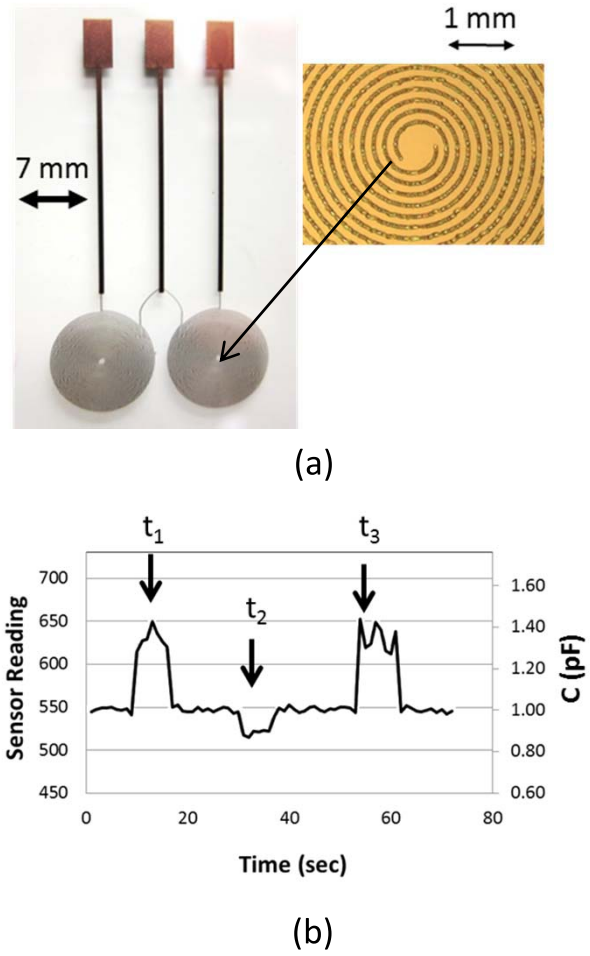

Fig. 7. (a) Photo images of a capacitive touch sensor made by double looped coils. The insert shows enlarged details of printed coils; (b) SL900A sensor reading of time sequence of finger touch test.

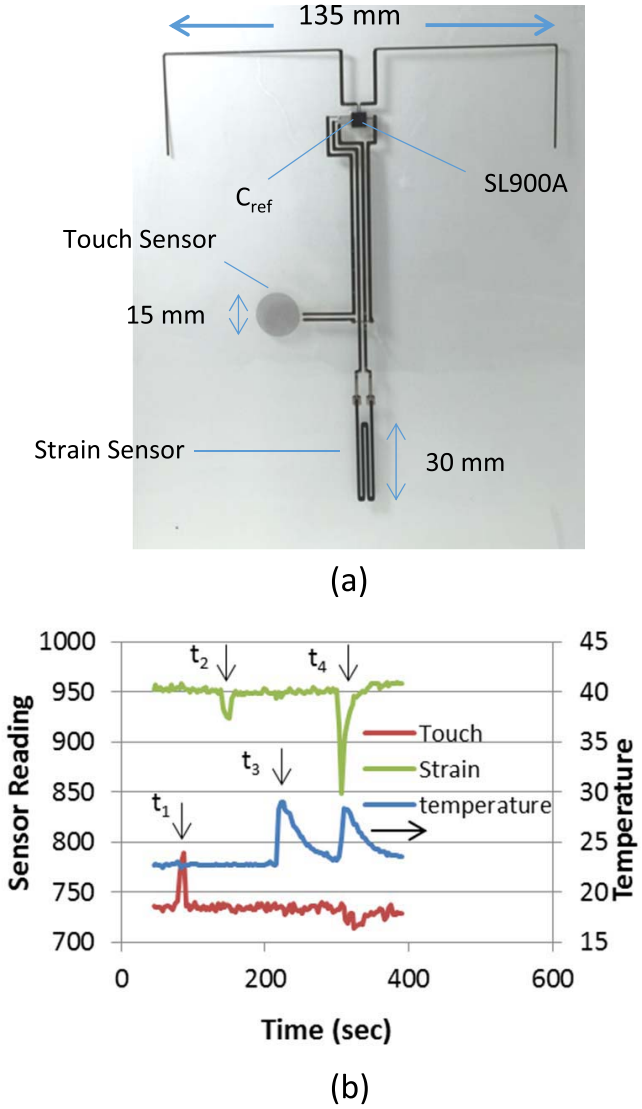

Fig. 8. (a) Photo image of an integrated sensor tag. (b) Examples of SL900A sensor reading.

digitally printed touch and strain sensors, antenna and interconnects. The sensor tag is fabricated on s 150 μm PEN substrate as shown Fig. 8(a). The antenna is made by extrusion printing of silver nanoparticle ink. The strain sensor is formed by extrusion printing of a resistive carbon ink and connected to the external sensor input EXT2 pin on the SL900A chip, as shown in the schematic of Fig 1 (b). The EXT2 sensor input on the reader is configured as conductance measurement. The touch sensor is made by aerosol jetted silver ink, as described in the previous sub section. There is a 10 pF surface mount discrete capacitor mounted by ACF as a reference capacitor and connected as in the schematic of Fig 1 (c). The EXT1 sensor input is configured as capacitance measurement. The packaged chip is bonded to the printed interconnects on the substrate with ACF.

Fig 8(b) shows an example of reading three sensor values from touch and strain sensors as well as the ambient temperature. To show touch sensing, a finger touched briefly on the sensing capacitor at time t_1, causing a positive capacitance change of ~7% (red curve). At time t_2, the strain sensor is under a tensile bending with bending radius of about 17 cm, the resistance of the strain sensor increases about 3%, and the reading shows a dip for the conductance value (green curve). The SL900A also contains an internal temperature sensor. The temperature reading is tested with a hot air gun (blue curve). At t_3, hot air is directed onto the chip and the reported temperature rises to ~30 °C. When hot air is directed to both chip and the strain sensor, the strain sensing value changes due to bending caused by the flowing air (150–500 liters/minute volumetric flow rate). However, with a similar bending radius, the resistance change is larger than that at room temperature (time t_4). This is mainly due to the temperature dependence of the resistance of the strain sensor and could be calibrated using the temperature reading. A small change in the capacitance reading is also noticed when the temperature is higher at time t_4.

V. Conclusion

In this paper we described our approach to combining digitally-printed components with Si IC chip for a wireless sensor system on a flexible substrate. The printed components include strain and touch sensors, antenna, and interconnects. An integrated printing system is developed for deposition

of versatile materials for different components. The IC chip performs RF communication, analogue to digital conversion, and energy harvesting. For chip attachment to a flexible substrate, we developed a method to planarize the die by embedding it within the volume of the substrate. This method enables direct connection between the contact pads of the die and the corresponding conductive traces on the substrate by printing conductive ink. Our approach facilitates customization to a wide variety of sensors and user interfaces suitable for a broad range of applications including remote monitoring of health, structures, and environment.

REFERENCES

[1] A. C. Arias, J. D. Mackenzie, I. McCulloch, J. Rivnay, and A. Salleo, "Materials and applications for large area electronics: Solution-based approaches," *Chem. Rev.*, vol. 110, no. 1, pp. 3–24, 2010.

[2] M. Jung *et al.*, "All-printed and roll-to-roll-printable 13.56-MHz-operated 1-bit RF tag on plastic foils," *IEEE Trans. Electron Devices*, vol. 57, no. 3, pp. 571–580, Mar. 2010.

[3] S. Khan, L. Lorenzelli, and R. S. Dahiya, "Technologies for printing sensors and electronics over large flexible substrates: A review," *IEEE Sensors J.*, vol. 15, no. 6, pp. 3164–3185, Jun. 2015.

[4] W. S. Wong and A. Salleo, "Flexible electronics materials and applications," in *Electronic Materials: Science & Technology*. New York, NY, USA: Springer. 2009.

[5] R. A. Street *et al.*, "From printed transistors to printed smart systems," *Proc. IEEE*, vol. 103, no. 4, pp. 607–618, Apr. 2015.

[6] K.-J. Baeg, M. Caironi, and Y.-Y. Noh, "Toward printed integrated circuits based on unipolar or ambipolar polymer semiconductors," *Adv. Mater.*, vol. 25, no. 31, pp. 4210–4244, 2013.

[7] E. Maiellaro *et al.*, "High-gain operational transconductance amplifiers in a printed complementary organic TFT technology on flexible foil," *IEEE Trans. Circuits Syst. I, Reg. Papers*, vol. 60, no. 12, pp. 3117–3125, Dec. 2013.

[8] T. S. Sekitani and T. Someya, "Stretchable, large-area organic electronics," *Adv. Mater.*, vol. 22, no. 20, pp. 2228–2246, 2010.

[9] B. Kang, W. H. Lee, and K. Cho, "Recent advances in organic transistor printing processes," *ACS Appl. Mater. Interfaces*, vol. 5, no. 7, pp. 2302–2315, 2013.

[10] T. N. Ng *et al.*, "Printed dose-recording tag based on organic complementary circuits and ferroelectric nonvolatile memories," *Sci. Rep.*, vol. 5, Aug. 2015, Art. no. 13457.

[11] T. N. Ng *et al.*, "Pulsed voltage multiplier based on printed organic devices," *Flexible Printed Electron.*, vol. 1, no. 1, p. 015002, 2016.

[12] L. Ruiz-Garcia, L. Lunadei, P. Barreiro, and J. I. Robla, "A review of wireless sensor technologies and applications in agriculture and food industry: State of the art and current trends," *Sensors*, vol. 9, no. 6, pp. 4728–4750, Jan. 2009.

[13] J. P. Lynch and K. J. Loh, "A summary review of wireless sensors and sensor networks for structural health monitoring," *Shock Vibrat. Dig.*, vol. 38, no. 2, pp. 91–128, 2006.

[14] E. J. Carlson, K. Strunz, and B. P. Otis, "A 20 mV input boost converter with efficient digital control for thermoelectric energy harvesting," *IEEE J. Solid-State Circuits*, vol. 45, no. 4, pp. 741–750, Apr. 2010.

[15] Y. Yang *et al.*, "Pyroelectric nanogenerators for harvesting thermoelectric energy," *Nano Lett.*, vol. 12, no. 6, pp. 2833–2838, 2012.

[16] T. M. Razykov, C. S. Ferekides, D. Morel, E. Stefanakos, H. S. Ullal, and H. M. Upadhyaya, "Solar photovoltaic electricity: Current status and future prospects," *Sol. Energy*, vol. 85, no. 8, pp. 1580–1608, 2011.

[17] P. D. Mitcheson, E. M. Yeatman, G. K. Rao, A. S. Holmes, and T. C. Green, "Energy harvesting from human and machine motion for wireless electronic devices," *Proc. IEEE*, vol. 96, no. 9, pp. 1457–1486, Sep. 2008.

[18] W.-C. Wang, L.-Y. Wu, L.-W. Chen, and C.-M. Liu, "Acoustic energy harvesting by piezoelectric curved beams in the cavity of a sonic crystal," *Smart Mater. Struct.*, vol. 19, no. 4, p. 045016, 2010.

[19] D. Patel, R. Mehta, R. Patwa, S. Thapar, and S. Chopra, "RF energy harvesting," *Int. J. Eng. Trends Technol.*, vol. 16, no. 8, pp. 382–385, 2014.

[20] D. E. Schwartz *et al.*, "Flexible hybrid electronic circuits and systems," *IEEE J. Emerg. Sel. Topics Circuits Syst.*, vol. 7, no. 1, pp. 27–37, Mar. 2016.

[21] R. Cauchois *et al.*, "Chip integration using inkjet-printed silver conductive tracks reinforced by electroless plating for flexible board packages," in *Proc. Micro/Noano-Electron. Packag. Assem. Design Manuf. Forum (MiNaPAD)*, Apr. 2012, pp. 1–5.

[22] *SL900A EPC Sensor Tag*. Accessed: Sep. 25, 2017. [Online]. Available: http://ams.com/eng/Products/Wireless-Connectivity/Sensor-Tags-Interfaces/SL900A

[23] M. A. Uddin, M. Y. Ali, and H. P. Chan, "Achieving optimum adhesion of conductive adhesive bonded flip-chip on flex packages," *Rev. Adv. Mater. Sci.*, vol. 21, no. 2, pp. 165–172, 2009.

[24] L. Xie, J. Shen, J. Mao, F. Jonsson, and L. Zheng, "Co-design of flip chip interconnection with anisotropic conductive adhesives and inkjet-printed circuits for paper-based RFID tags," in *Proc. IEEE 61st Electron. Compon. Technol. Conf.*, May/Jun. 2011, pp. 1752–1757.

[25] T. Zhang *et al.*, "Flexible electronics: Thin silicon die on flexible substrates," *IEEE Trans. Electron. Packag. Manuf.*, vol. 32, no. 4, pp. 291–300, Oct. 2009.

[26] S. Yang and N. Lu, "Gauge factor and stretchability of silicon-on-polymer strain gauges," *Sensors*, vol. 13, no. 7, pp. 8577–8594, 2013.

Ping Mei received the B.S. degree in physics from Rutgers University, New Brunswick, NJ, USA, and the Ph.D. degree in physics from Peking University, Beijing, China.

From 1992 to 2001, she was with the Palo Alto Research Center (PARC), when she studied and developed various techniques for amorphous Si and poly-Si TFT fabrication, especially laser crystallization and laser doping techniques for flat panel imaging applications. In 2001, she joined Hewlett Packard Labs on a quest to develop roll-to-roll fabrication process for building electronic devices on flexible substrates. She co-invented and developed self-aligned imprint lithography for flexible display backplane. In 2013, she returned to PARC. Her current research interests include integration of printed components with wireless communication chips on flexible substrates for smart sensor applications.

Brent Krusor received the B.S. degree in chemistry from MIT and the M.S. degree in physical chemistry from the University of California at Berkeley. He is a member of the Printed Electronic Devices Group, which focuses on inkjet printing of organic electronic materials to create flexible, large-area transistor, and sensor arrays. Since joining PARC in 1978, he has worked in the areas of molecular beam epitaxy of III-V semiconductors, high-resolution X-ray diffraction, and magneto-optical memory technology.

He has authored over 30 technical papers and is a co-inventor of 13 issued U.S. patents.

David E. Schwartz received the B.S. degree in mathematics from Brown University, Providence, RI, USA, in 1997, and the Ph.D. degree in electrical engineering from Columbia University, New York, NY, USA, in 2008. He is the Manager of the Energy Devices and Systems area at PARC, and he serves as the Lead Circuit and System Designer for PARC's printed and hybrid electronics programs.

Tse Nga Ng received the M.S. and Ph.D. degrees in physical chemistry from Cornell University, Ithaca, NY, USA, in 2002 and 2006, respectively, where she worked with Prof. J. Marohn. Subsequently, she joined the Palo Alto Research Center, Palo Alto, CA, USA. Since 2015, she has been an Associate Professor with the Electrical and Computer Engineering Department, University of California at San Diego. Her research has focused on flexible printed electronics, including bendable image sensors for X-ray medical imaging and additive processes for integrated sensor tags. Her work on printed systems received the 2012 Innovation Award from Flextech Alliance and has been named Runner-up for the Wall Street Journal Technology Innovation Award.

George Daniel is a VP of Engineering of Metawave and a Senior RF Engineering Architect with more than 30 years' experience working in the advanced development groups of Sony Ericsson and GE Radar Systems. Prior to joining Metawave, he was Senior RF Engineer at Xerox PARC, engaged in applied electromagnetic technology research, analysis, design, implementation, and testing for over a dozen technologies. Before PARC, he was a Co-Founder and the President of Accurate Electronics—an engineering firm that integrated wireless capability into GE Energy's smart meters antenna design, and redesigned GE Energy's flagship product's main metrology assembly. His areas of expertise include metamaterials in the microwave and mm-wave bands, wireless communication, transceiver architecture, sensor networks, power conversion, antenna design, and radar systems.

Steve Ready has designed and developed several highly accurate and versatile printers for printed electronics and 3-D smart objects; studied the role of hydrogen in amorphous, polycrystalline and crystalline silicon and associated applications; contributed to the development of large-area amorphous and polycrystalline silicon arrays for optical and x-ray imaging and also display technology since joining the Palo Alto Research Center over three decades ago. He has had the opportunity to give several invited talks at international conferences on printed electronics and 3-D silicon technology.

Gregory L. Whiting was born in Edinburgh, U.K. in 1979. He received the B.S. degree in chemistry from the University of California at Berkeley in 2002, and the Ph.D. degree in chemistry from the University of Cambridge in 2007.

He was with a number of organizations including Cambridge Display Technology from 2006 to 2008, the Palo Alto Research Center from 2008 to 2016, and Google[X] from 2016 to 2017, prior to his current position as an Associate Professor with the Mechanical Engineering Department, University of Colorado Boulder. His research interests include additive and digital manufacturing, printed and flexible electronics, transient electronics and distributed systems for application in areas, including health care, robotics, data security, and waste reduction.

He has co-authored over 20 peer-reviewed journal articles and holds over 25 U.S. patents. He has received a number of awards including the FlexTech Alliasnce Flexi Award and the Top Performer Award from DARPA. He is a 2016 National Academy of Engineering Frontiers of Engineering Participant.